Phase Change Material with Gelation Imparting Shape Stability

Gleb Vasilyev,* Naama Koifman, Michael Shuster, Michael Gishvoliner, Yachin Cohen, and Eyal Zussman*

Read Online

ACCESS | Metrics & More | Article Recommendations | Supporting Information

ABSTRACT: Blending two gelators with different chemistries (12-hydroxystearic acid and a bis-urea derivative, Millithix MT-800) was used to impart shape stability to CrodaTherm 29, a bio-based phase change material (PCM), melting/crystallizing at near-ambient temperature. The gelators immobilized the PCM by forming an interpenetrating fibrillar network. 15 wt % concentration of the gelators was found to be effective in preventing liquid PCM leakage. In order to improve the mechanical properties and thermal conductivity (TC) of the PCM, gelation of suspensions of multiwalled carbon nanotubes (MWCNTs) and graphene nano-platelets (GnPs) in a molten material was done at concentrations exceeding their percolation thresholds. Compared to pristine PCM, the gelled PCM containing 3.0 wt % of GnPs demonstrated a shorter crystallization time, ∼1.5-fold increase in strength, improved stability, and ∼65% increase in TC. At the same time, PCM filled with up to 0.6 wt % of MWCNTs had diminished strength and increased leakage with a slight TC improvement. Gelation of PCM did not significantly alter its thermal behavior, but it did change its crystalline morphology. The developed shape-stable PCMs may have a wide range of applications in ambient temperature solar-thermal installations, for example, temperature-controlled greenhouses, net zero-energy buildings, and water heaters.
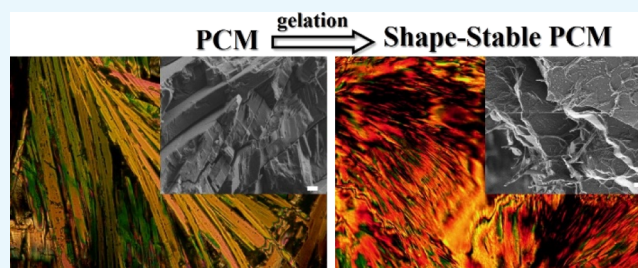
1. INTRODUCTION

The need for energy efficiency and the increase in energy consumption have prompted an interest in phase change materials (PCMs) as a thermal energy storage system.[1,2] Upon heating, PCMs undergo melting, absorbing a large amount of thermal energy in the form of latent heat, which can be released during crystallization.

Organic PCMs, such as paraffins, alcohols or polyalcohols, fatty acids, and their derivatives, are of special interest due to their low corrosivity, congruent melting, crystallization behavior, relatively high latent heat of phase transition, good thermal and chemical stability, and a wide range of phase-transition temperatures.[3] Despite this, PCMs are limited in their practical use in technical applications because they tend to leak into the environment after undergoing solid−liquid transition, raising demands for shape-stable PCMs (SSPCMs).

There are several strategies for imparting shape stability to organic PCMs. Shape stabilization, for instance, can be achieved by confining PCMs in a polymer matrix. Different polymers, including polyethylenes[4−6] and block copolymers,[7−10] were used for this purpose. However, in many cases, complete prevention of the leakage could be achieved at a rather high polymer concentration of 25−30%, thus resulting in significant latent heat loss. Another approach is creating a fine internal network scaffold, which immobilizes molten PCM and prevents leakage. As an example, a palmitic acid-based PCM can be prepared by in situ polymerization of castor oil.[11]

The castor oil formed a network, and a maximum palmitic acid immobilization ratio of 70% was obtained. Within the prepared SSPCM, immobilized palmitic acid exhibited a slightly distorted crystalline structure compared to the pristine form. As a result, heat of fusion and crystallization of the immobilized palmitic acid decreased, and its contribution to latent heat storage capacity of the SSPCM was lower than that expected from the additivity rule: equivalent to ∼64% rather than 70% content.

According to a recent study, a polymer matrix combined with gelators can impart shape stability to organic PCMs.[12] Gelation restricted polymer mobility, improved melt process-ability, and controlled in situ self-assembly, resulting in a PCM content of up to ∼78%. In another study, hydroxypropyl cellulose was used as a gelling agent to prepare a SSPCM comprising a binary eutectic mixture of methyl palmitate and lauric acid as the thermal energy storing component.[13] The optimum gelator concentration that provides good shape stability was found to be 10 wt %. Gelation of the PCM did not cause any phase separation or incongruent melting. However,
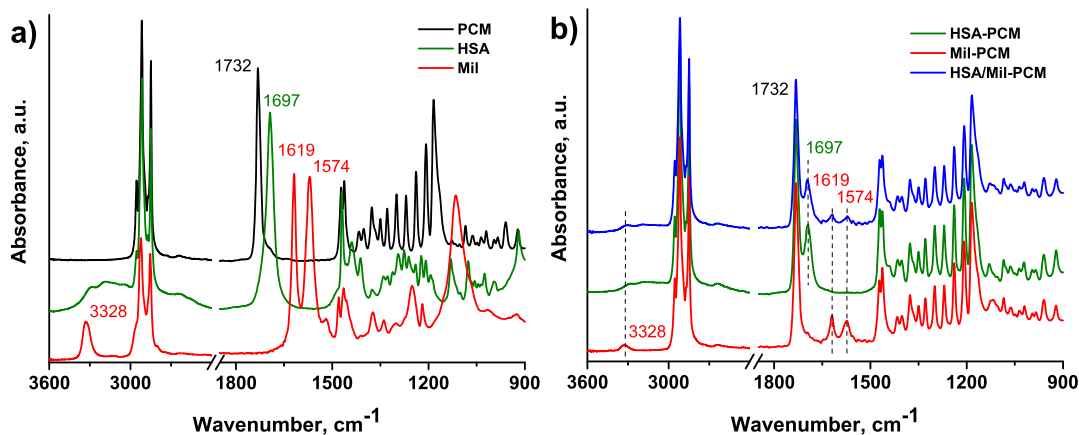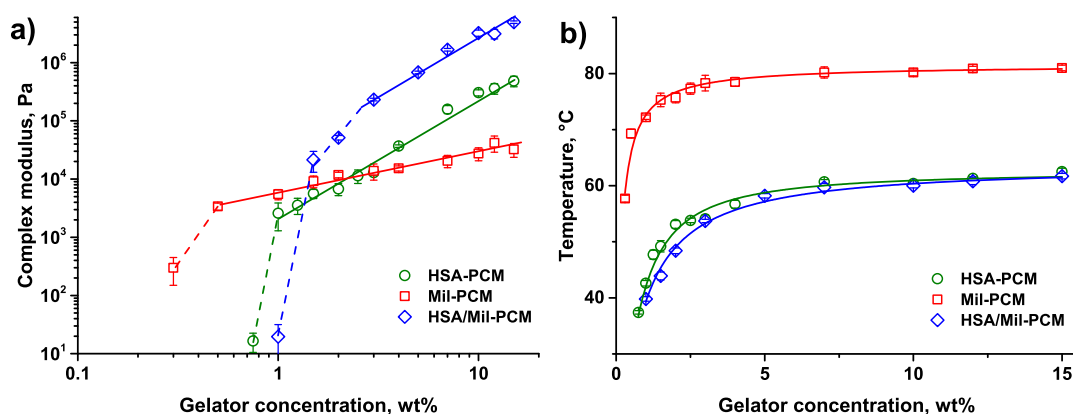
Figure 1. FTIR spectra of (a) pristine PCM and gelator, HSA and Mil, and powders; (b) HSA-, Mil-, and HSA/Mil-PCM gels. The spectra were collected at the temperature corresponding to the completion of both gelation and PCM crystallization.

Figure 2. Concentration dependence of: (a) complex modulus after incubation at 30 °C for 35 min and (b) gel−sol transition temperature for HSA-, Mil-, and HSA/Mil-PCM gels. The data for gels with low gelators' concentration (up to 3 wt %) are taken from our previous publication.[23]

the melting temperature of the SSPCM slightly shifted toward lower temperatures, and the heat of fusion was ∼13% lower than that expected from the additivity rule. The ability of dibenzylidene sorbitol (DBS) derivatives to gel different organic PCMs was also demonstrated.[14] This organogelator formed a thermo-reversible fibrillar network in both polar and non-polar molten PCMs. The polar PCMs contained thinner gelator fibrils organized in a denser network, resulting in a weaker leakage of the molten PCM. Complete suppression of leakage was achieved at ∼15 wt % of DBS, and the loss in heat of fusion and crystallization of PCM was slightly lower than the values calculated according to the weight fraction of the PCM.[15]

The use of solid micro- or nanoparticles is another popular way to impart shape stability to PCMs.[16−19] Being properly dispersed, at the percolation threshold concentration, the particles form a continuous network, supporting and immobilizing molten PCMs and hampering their leakage. The percolation threshold value is strongly dependent on the particle size and geometry.[20] It decreases with size and increases in the order of rods < platelets < spheres. Using carbonaceous micro- or nanoparticles with high thermal conductivity (TC), such as carbon nanotubes, graphene, or graphite, which have high TC, the thermal performance of SSPCMs can be improved significantly.[21,22]

In our previous work,[23] we reported the ability of 12-hydroxystearic acid (HSA) and a commercially available bis-

urea derivative, Millithix MT-800 (Mil), which are well-known gelators, for a wide range of both polar and non-polar organic fluids,[24−27] to gel a bio-based organic PCM. Blends of these two gelators taken in different proportions were also capable of gelling the molten PCM. Moreover, a strong synergistic effect at a HSA/Mil ratio of 83/17 wt % was found. Particularly, the two gelators blended in this proportion provided gels with ∼20-fold higher modulus than each gelator individually. As the modulus value for the gels was almost frequency independent, it could be treated as a plateau modulus, which is directly related to the mesh size or density of the network formed in the system.[28] In fact, this means that the gel based on the blended gelator with a HSA/Mil ratio of 83/17 wt % has the densest network. Because the high density of a network is one of the most important requirements for effective immobilization of fluids, we considered this formulation as a promising candidate for SSPCM fabrication, hence focusing the present study on gels with a fixed HSA/Mil ratio of 83/17 wt %. By varying the total gelator concentration at the fixed HSA/Mil ratio, an SSPCM gel was prepared, with no evident PCM leakage. Thermal and thermo-mechanical properties of the SSPCM gel, as well as the effect of the blended gelator on the crystalline structure of the PCM, were examined. In addition, in order to improve the TC of the SSPCM, composite SSPCMs, containing multiwalled carbon nanotubes (MWCNTs) or graphene nanoplatelets (GnPs), were fabricated and characterized.

2. RESULTS AND DISCUSSION

2.1. PCM Gels. First, specific molecular interactions between the gelators and the PCM were examined, as these interactions can strongly influence the phase behavior of both gelling agents and PCM.[29,30] The PCM used in this study is known to be fatty acid-derived and indeed the Fourier-transform infrared (FTIR) spectrum of the PCM powder showed a high-intensity band at 1732 cm^{-1}, corresponding to stretching vibrations of C=O in carboxyl groups (Figure 1a), which can potentially partake in hydrogen bonding with the carboxyl groups of HSA and/or carbonyl or amine groups of Mil. However, both HSA and Mil spectra within the corresponding PCM gels were identical to those of the pure gelators. Moreover, the spectrum of HSA/Mil-PCM gel could be represented as a combination of pure HSA, Mil, and the PCM spectra, strongly suggesting no hydrogen bonding between the three gel constituents. Positions of all characteristic bands, that is, at 3000−3400 cm^{-1} (the region related to hydrogen bonding between the hydroxyl groups) and 1697 cm^{-1} (hydrogen-bonded carboxyl groups) for HSA[31] as well as 3328 cm^{-1} (NH stretching vibrations), 1619 cm^{-1} (amide I), and 1574 cm^{-1} (amide II) for bis-ureas,[32] remained unchanged, confirming the absence of specific interactions between the gelling agents and PCM (Figure 1b).

At concentrations above a certain critical value, both individual HSA, Mil, and HSA/Mil blend were capable of immobilizing the liquid PCM due to continuous fibrillar network formation. Figure 2a presents plots of complex modulus, G^*, versus concentration of the gelling agents for the gels. The plots show a linear increase of G^* with concentrations over a wide concentration range. At the lowest tested HSA and Mil concentration, the linearity does not hold anymore, with G^* values significantly lower than the linear trend would suggest, implying the formation of isolated fibrillar clusters rather than a continuous network by the gelators in 0.3% Mil-PCM and 0.75% HSA-PCM formulations. A similar pattern is observed for the blended HSA/Mil gelator containing gels. However, the deviation from linearity (transition from the separated clusters to a continuous network) starts at a higher gelator concentration and occurs more gradually, over a wider gelator concentration range (of ~1.5−3 wt %).

Linear segments of the concentration dependencies for HSA- and Mil-PCM gels differ in their slopes. For Mil-PCM gels, the slope is rather low, that is, 0.75. Similarly, a low exponent value of 0.8 was found for gels of a DBS derivative in several liquids with high gelator concentrations. It was ascribed to the aggregation of individual networks forming fibrils into bundles as the concentration increased.[33] For HSA-PCM gels, the slope was ~1.9, which is similar to the values reported for other existing gels,[34,35] and close to the theoretical value of 2.0 derived for rigid networks formed by cross-linked rigid fibrils.[36] In the concentration range, corresponding to the continuous network existence, the slope of the dependence for HSA/Mil-PCM gels was the same (~1.9) as that for HSA-PCM gels. However, the absolute G^* values for HSA/Mil-PCM gels were approximately 20-fold higher than those for HSA-PCM gels. The difference is practically concentration independent. Similar synergistic effects have been previously reported for several gels with multicomponent gelators, such as co-assembled peptides,[37] a blend of long-chain alkylamides,[38]

self-sorted chiral phenylalanine-based hydrogelators,[39] and self-sorted derivatives of DBS.[40]

The concentration dependencies of the gel−sol transition temperature, T_{g-s} (Figure 2b), for all three series exhibited typical phase-transition temperature behavior.[41] At each fixed gelator concentration, absolute values of T_{g-s} for Mil-PCM gels were 20−25 °C higher than those of HSA-PCM gels. At the same time, T_{g-s} for HSA/Mil-PCM gels were just 2−5 °C lower than those of HSA-PCM gels over the entire range of the concentration tested.

Considered together, these concentration dependencies of G^* and T_{g-s} suggest that mainly HSA determines and is responsible for thermal stability and mechanical properties of HSA/Mil-PCM gels at a HSA/Mil ratio of 83/17, while the presence of Mil provides the synergistic effect.

2.2. Shape-Stable and Composite PCMs. *2.2.1. Leakage of Molten PCM.* Proper immobilization of PCM and complete suppression of its leakage in the surroundings following the solid−liquid phase transition is one of the most important requirements for SSPCMs. To characterize shape stability, leakage of the PCM from HSA/Mil-PCM gels soaked at 42 °C for 2 h was examined. Figure 3 presents the leakage as a
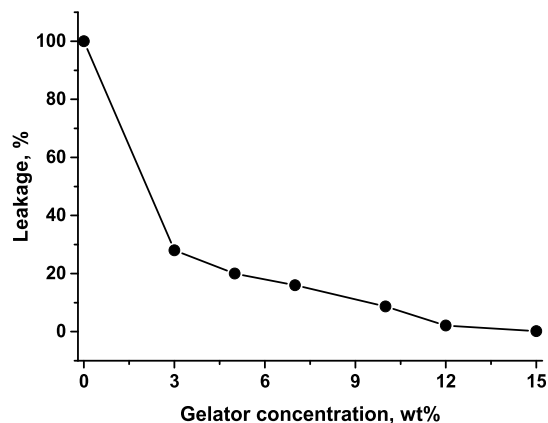
Figure 3. Leakage of PCM soaked at 42 °C for 2 h as a function of gelator concentration in HSA/Mil-PCM gels.

function of the gelator concentration. The lowest HSA/Mil gelator concentration selected for testing was 3 wt %, assuming the critical concentration of continuous gelator network formation (or close to that). Leakage at this concentration was unacceptably high ~30%. The leakage progressively decreased as the gelator concentration increased, and the almost complete suppression of the PCM leakage was achieved at a gelator concentration of 15 wt %. Thus, the HSA/Mil-PCM gel with a 15 wt % gelator concentration was treated as the SSPCM and this formulation was used for composite SSPCM preparation.

The low TC of organic PCMs is a major drawback of these materials. Serious efforts are being spent on improving this property. The improvement can be achieved by incorporation of highly thermally conductive materials in PCM formulations, resulting in composite PCM formation. For example, various carbonaceous particles (graphite, graphene, or carbon nanotubes) are widely used.[42] To be effective, thermally conductive fillers should form a network of particles being in direct contact with each other. The critical concentration of the particles allowing network formation (percolation threshold) depends both on the particles' geometry and their dispersion state.

Besides providing enhanced TC, the network of filler particles may also contribute to the shape stability of PCM, suppressing its leakage and serving as a supporting component of the material. In this way, incorporation of carbonaceous fillers may facilitate the optimization of SSPCM formulations.[43]

Aiming at TC improvement, two series of composite SSPCM containing various concentrations of either MWCNTs or GnPs and a fixed (15 wt %) HSA/Mil-blended gelator concentration were prepared. The concentration of MWCNTs in the composite SSPCM varied in the range of 0.2−0.6 wt %, whereas that of GnPs was within the 0.5−3.0 wt % range. The upper limit of the concentrations was stipulated by the difficulties in the preparation and processing of the PCM−filler suspensions. Above this limit, shortly after the beginning of sonication, the liquid-like suspensions transformed into slurry-like materials, making further treatment inefficient. Moreover, subsequent addition, dissolution, and homogenization of the gelators in the heated suspensions was hampered. Progressive incorporation of the carbonaceous fillers caused the rheological response of molten SSPCM to transform into viscoplastic behavior, typical for composites.[44] Molten composite gels with the highest filler loadings demonstrated this behavior most clearly; hence, they were the focus of further study. At the highest concentrations used, 0.6 and 3.0 wt % for MWCNTs and GnPs, respectively, the composite SSPCMs in the molten state manifest pronounced yielding, whereas SSPCM without fillers behaves as a low-viscosity Newtonian fluid (Figure 4).
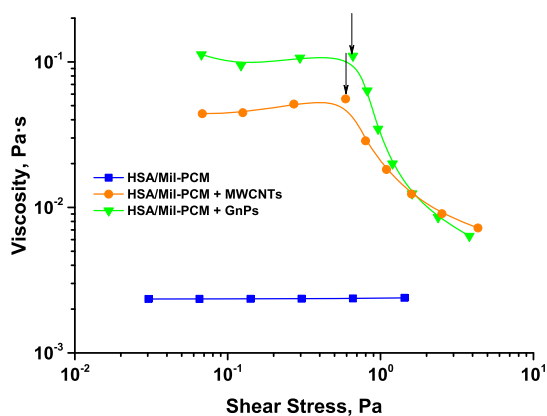
Figure 4. Flow curves of SSPCM (15 wt % HSA/Mil-PCM) and composite SSPCMs containing either 0.6 wt % of MWCNTs or 3.0 wt % of GnPs in the molten state (110 °C). Arrows point to the yield stress.

Within the range of the studied shear stresses and rates, both molten composite SSPCMs demonstrate similar flow behavior. They exhibit quite high yield stress values of 0.6 and 0.65 Pa for composite SSPCMs with MWCNTs and GnPs, respectively, confirming the presence of a continuous structure formed by the filler particles.

Despite the presence of a continuous filler particle network, MWCNTs containing SSPCMs exhibited a PCM leakage of 1−3% for all formulations (Figure 5). Composite SSPCM containing GnPs particles showed similar and even stronger leakage at the lowest filler content. However, the leakage decreased at higher GnP concentration, and almost no PCM leakage was detected for the 3 wt % GnP composite SSPCM. It has to be mentioned that the leakage degree was not exactly 0% for all of the samples (Table S1). Apparently, an external
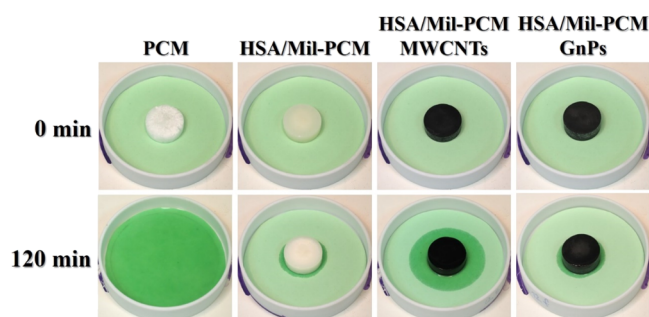

**Figure 5.** Digital images of samples before and after leakage tests.

surface (facets, which were in contact with the mold surface) of the samples used for the test contained some amount of unconstrained PCM, which leaked away after the PCM was melted. As observed for HSA/Mil-PCM and 3 wt % GnP composite SSPCM this portion of PCM was very low and provided a contribution of ∼0.2%, which could be considered negligible. However, for MWCNTs containing SSPCMs, the leakage was significantly stronger and hence should be ascribed to the effect of the composite structure.

2.2.2. Microscopic Study. Figure 6 shows light microscopy images of the blended gelator HSA/Mil-PCM gel and images of individual gelators, HSA- and Mil-PCM gels, of the same (15 wt %) concentration. Continuous fibrillar networks are clearly seen in all images. However, the morphology of the networks is different. Two distinct types of network-forming fibrils are present in the HSA-PCM gel (Figure 6a). The first network is characterized by sparse fibrils that appear thick, very long, and only slightly curved, indicating their rigidity. Meanwhile, HSA fibrils are thinner and shorter, creating a continuous dense network. Under crossed polarizers, fibrils, especially thick ones, show birefringence, indicating their crystalline structure (Figure 6d). Similarly, the Mil-PCM gel shows a hierarchical distribution of fibrils (Figure 6b). However, unlike HSA, thick Mil fibrils are much more curved and tend to form elliptical structures, suggesting their higher flexibility. Thin Mil fibrils are so small that they can hardly be detected by light microscopy and are much less birefringent than the HSA ones (Figure 6e). Two populations of network forming fibrils differing in thickness are also seen in a blended gelator HSA/Mil-PCM gel (Figure 6c). Compared with HSA- and Mil-PCM gels, the HSA/Mil-PCM gel network shows a higher proportion of thick fibrils. As a result, the network appears to be significantly denser. The fibrils are well entangled, quite long (though shorter than thick fibrils in the pure HSA-PCM gel), flexible, and sometimes branched. A few large aggregates are seen in the image. Birefringence of thick fibrils, building the network in the gels decreases in the following order: HSA- > HSA/Mil- > Mil- (see Figure 6d−f).

Cryo-SEM imaging was carried out to get further insights into the microstructure of the HSA/Mil-PCM gel. It was shown that in the molten PCM, HSA forms both helical and double helical fibrils, while Mil fibrils are significantly thinner, untwisted, and smooth.[23] Both HSA- and Mil-type fibrils were found to coexist in the bulk of the HSA/Mil-PCM gel. Predominantly, they were uniformly distributed and bundled, forming a dense network (Figure 7a,b). However, regions containing only characteristic helical fibrils (HSA) were also found. In these regions, the fibrils were closely packed, looking like aggregates.
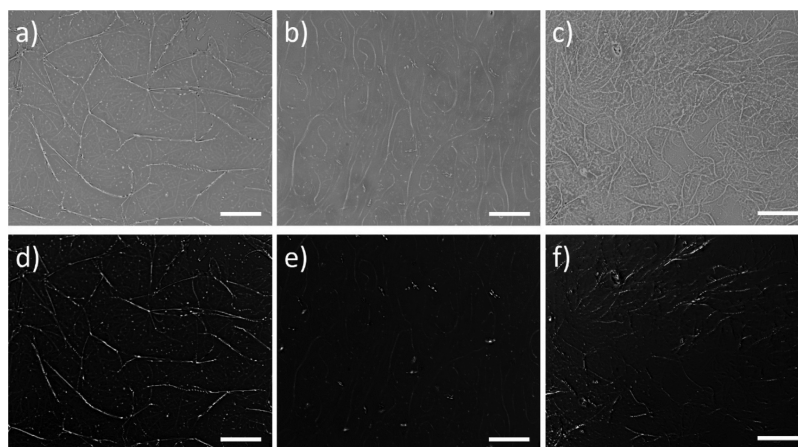
Figure 6. Light microscopy images of 15 wt % (a,d) HSA-PCM, (b,e) Mil-PCM, and (c,f) HSA/Mil-PCM gels in (a−c) bright-field and (d−f) polarized light modes. Scale bars represent 50 μm. The images were captured at a temperature exceeding the melting point of the pure PCM.
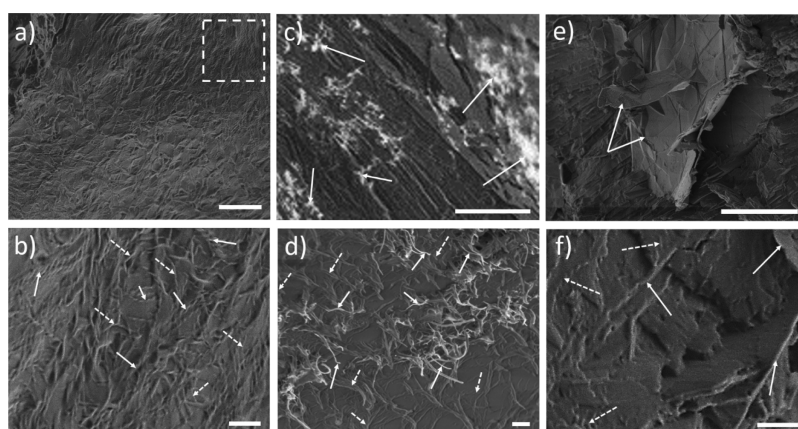

Figure 7. Cryo-SEM images of (a,b) HSA/Mil-PCM gel and the composite SSPCM containing (c,d) MWCNTs and (e,f) GnPs at (a,c,e) low and (b,d,f) high magnifications. In (b), networks of well-dispersed HSA (solid arrows) and Mil (dash arrows) fibrils are shown. Dash rectangle in (a) depicts an aggregate formed by HSA fibrils. In (c−f), dashed and solid arrows point to gelator fibrils and filler particles or their aggregates, respectively. The latter (especially MWCNTs) appears brighter in a secondary electron image, given the fillers are conductive, while the PCM is an insulator.[45] Scale bars represent 2 μm in image (a), 10 μm in images (c,e), and 400 nm in images (b,d,f).
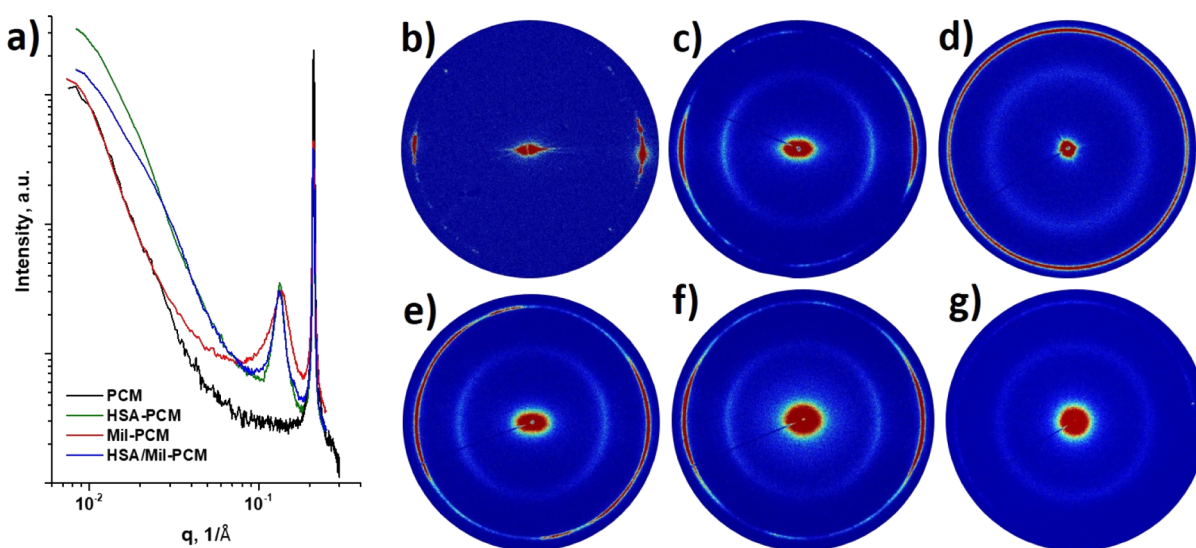
Figure 8. (a) SAXS curves of PCM, 15 wt % HSA-, Mil-, and HSA/Mil-PCM gels at 20 °C. 2D SAXS patterns: (b) PCM, (c) HSA-PCM, (d) Mil-PCM, and (e) HSA/Mil-PCM gels and the composite SSPCM containing (f) MWCNTs and (g) GnPs.
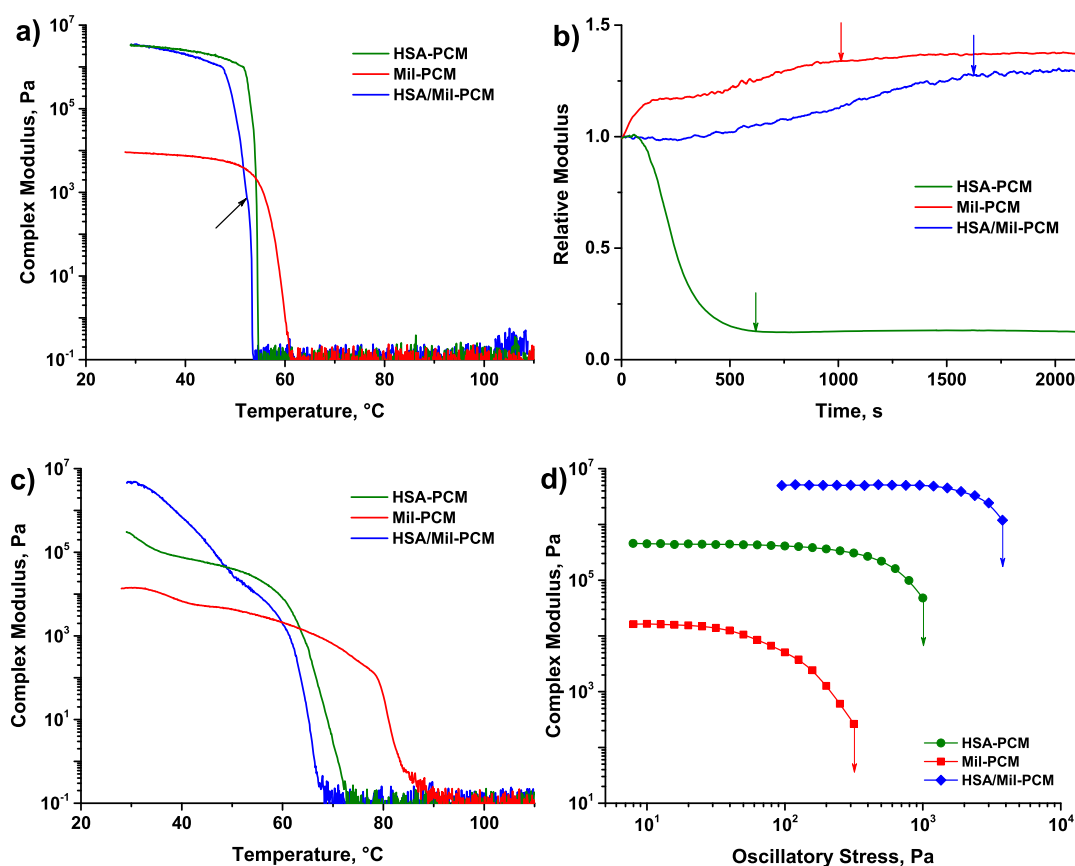
Figure 9. Typical dependences of the complex modulus vs temperature during (a) cooling and (c) heating stages; (b) evolution of the relative complex modulus over time during incubation at 30 °C for 15 wt % HSA/Mil-PCM gel and for single-component HSA- and Mil-PCM gels of the same effective gelator concentrations (12.5 and 2.5 wt % for HSA and Mil, respectively); and (d) complex modulus versus oscillatory stress amplitude at 30 °C and a frequency of 1 Hz for 15 wt % HSA-, Mil-, and HSA/Mil-PCM gels.

Both fillers, MWCNT and GnP, were dispersed within the PCM matrix unevenly, being present as individual particles, quite big aggregates, bundles, and stacks (Figure 7c−f). The introduction of the particles did not introduce any new chemical interactions between the constituents of the SSPCMs (PCM, HSA, and Mil) as the FTIR spectrum of the original HSA/Mil-PCM and those of composite SSPCMs are practically identical (Figure S1).

2.2.3. Crystalline Microstructure. Crystalline phase organization was studied using small-angle X-ray scattering (SAXS) experiments. Figure 8a shows SAXS results for pure PCM, 15 wt % HSA-, Mil-, and HSA/Mil-PCM gels at 20 °C, when the gels are crystalline solids. A single narrow scattering peak at 0.212 Å^{-1}, corresponding to a spacing of 3.0 nm was registered for the neat PCM. Well-reasoned ascribing of the peak to the fine organization of PCM molecules was impossible because their exact chemical structure remains unclear. It is, however, close to the (001) reflection of isopalmitic acid.[46] It thus stands to reason that this is a long-period reflection of a fatty acid-layered crystal. This reflection appears in Figure 8b as arcs centered on the equator, indicating the orientation direction of the crystal's long period, which is usually related to the direction perpendicular to the crystalline layered structure. The diffuse SAXS pattern from the PCM at very low angles, as seen at the center of Figure 8b, is elliptic with the long axis along the equator, the direction of the crystal's long period. This indicates that the crystal structures are highly anisotropic, most like thin platelets, perpendicular to the equatorial direction.

Two distinctive scattering peaks at 0.134 and 0.212 Å^{-1}, corresponding to spacings of 4.7 and 3.0 nm, respectively, are detected for the HSA-PCM, as shown in Figure 8c. The former peak corresponds to the (001) Bragg reflection of the HSA crystal.[47,48] The second peak represents periodicity in the PCM structure. Because the position of the corresponding peaks of pure and gelled PCM remains unchanged, it follows that the HSA network, formed during gelation, does not significantly affect the crystalline structure of the PCM at the nanometer scale. Both reflections appear as equatorial arcs, yet with a wider azimuthal breadth, as well as an elliptic equatorial diffuse SAXS pattern. This indicates that the HSA fibrils have some measure of preferential orientation and that the HSA crystal's long period (001) direction is parallel to that of the PCM. It has been reported that the HSA fibril axis in organogels is perpendicular to the (001) axis.[49] Two peaks at exactly the same positions were also found for Mil-PCM. Periodicity in the Mil crystalline structure at a nanometer scale gave rise to X-ray scattering at the same angle as the scattering from the (001) plane in the HSA crystal. Therefore, we were unable to distinguish between the contributions of the constituents, HSA and Mil, to the structure of blended gelator crystalline SSPCM. However, the qualitative difference in the effect of the gelator network on the structures formed in solidified HSA- and Mil-PCM gels is evident. Whereas in HSA-PCM gels both components exhibit a preferred orientation upon the completion of both gelation and PCM crystallization, with their long period in the same direction, the Mil-PCM

SAXS patterns are isotropic indicating no preferential orientation of either Mil or PCM (Figure 8d). The origin of the structural orientation in the PCM and HSA-PCM samples probably lies in the preparation technique, which includes controlled cooling of the gels and crystallization between parallel plates of a rotational rheometer. It appears that the HSA network does not prevent PCM-oriented crystallization; moreover, it helps to preserve this orientation in time. In contrast, the Mil network either impedes PCM-oriented crystallization or facilitates its reorganization.

The presence of the fillers influenced the organization of PCM crystallites in the composite SSPCMs. Incorporation of the particles suppressed the preferential orientation of both PCM and gelator fibrils detected for the SSPCM. The 2D SAXS pattern of MWCNT containing composite SSPCMs is similar to that of the unfilled SSPCM, and only a slight decrease in the intensities of the arcs, reflecting the preferential orientation of PCMs and gelator fibrils, was detected (compared to Figure 8e,f), indicating a lower orientation degree. In contrast, the 2D SAXS pattern of GnPs containing composite SSPCMs demonstrates uniform diffuse rings rather than arcs (Figure 8g), indicating no preferential orientation of either gelator fibrils or PCM crystals.

2.2.4. Rheological Properties. Thermo-mechanical behavior of the HSA/Mil-PCM gel was characterized using oscillatory rheometry. Figure 9a presents typical plots of a complex modulus as a function of temperature, recorded on cooling. The corresponding curves for individual gelator HSA- and Mil-PCM gels of the same effective gelator concentration (12.5 and 2.5 wt % for HSA and Mil, respectively) are also presented for comparison. The cooling steps started at 110 °C. At this temperature, $G*$ of all gels is so low that no differences in their rheological behavior can be detected. As the temperature goes down, $G*$ of the gels does not change until a critical temperature, T_{s-g}, which is different for different gels, was reached (see Figure 9a). A steep growth (several orders in magnitude) of $G*$ is observed at this critical temperature. This effect is associated with a rapid and massive network formation, and the slope of the rising segments reflects the kinetics of the network building up under non-isothermal conditions. The slope values were determined to be 9.8, 1.1, and 6.6 for HSA-, Mil-, and HSA/Mil-PCM gels, respectively, whereas the corresponding critical temperatures are 54.9, 61.2, and 53.6 °C. Comparing thermo-mechanical behavior of the gels, one can conclude that in terms of the network formation temperature and kinetics, the HSA/Mil-PCM gel is very similar to the HSA-PCM gel, implying its gelation starts with the HSA network formation. Kinetics of network formation in the HSA/Mil-PCM gel is significantly slower than that of the single-gelator HSA-PCM gel of the same effective concentration, as evidenced by the lower slope of the $G*$ versus temperature segments (6.6 vs 9.8). Also, the presence of Mil slightly delayed gelation by HSA, as the T_{s-g} shifted toward low temperatures (from 54.9 to 53.6 °C). Unlike individual gelator gels, the rising segment of $G*$ versus temperature plot for the blended gelator gel demonstrates an inflection point at ~52.3 °C (pointed by an arrow), slightly below the onset of the HSA network formation temperature. This inflection point, indicating a transition from fast network formation kinetics to more slow kinetics, is most likely associated with the onset of Mil network formation. Similar to the effect of Mil presence on gelation by HSA, the presence of HSA decelerates and delays Mil network formation. Particularly, the slope, reflecting

kinetics of the Mil network formation decreased from 1.1 (in Mil-PCM) to 0.95. The onset of the Mil network formation shifted significantly toward lower temperatures (from 61.2 °C in Mil-PCM to 52.3 °C in HSA/Mil-PCM) because of low Mil fraction (17 wt %) in the HSA/Mil blend. Thus, the equilibrium network formation in the blended gelator gel is a complex process, with each of the gelators building up their own fibrillar structures concurrently, forming interpenetrated networks.

The accomplishment of equilibrium network formation, evidenced by $G*$ stability in time at the final fixed temperature, is a slow process. After the cooling stage, network formation and reorganization were still ongoing, requiring an isothermal incubation stage at 30 °C. Figure 9b shows the progress of the network formation during the incubation step, expressed as the evolution of a relative modulus (current complex modulus normalized by the modulus at the beginning of the incubation stage) over time. Blended gelator HSA/Mil-PCM and Mil-PCM gels behaved similarly during the incubation stage. The gradual modulus increase in time was observed for both gels, followed by leveling off and reaching a plateau (indicated by arrows) with the moduli 1.2−1.3 times higher than the initial value. For the HSA/Mil-PCM gel, the process of network completion during the incubation step was slower than that for the Mil-PCM gel of the same effective concentration, requiring ~25 and ~15 min, respectively. In contrast, the HSA-PCM gel demonstrated instability in time with a significant, ~6-fold, modulus drop. Evidently, the presence of the Mil network stabilizes the HSA network, preventing rearrangements of its structure, accompanied by the modulus decrease.

Figure 9c presents typical plots of $G*$ as a function of temperature, recorded on heating. At the initial stages of heating, both HSA- and Mil-PCM gels demonstrated a moderate modulus decrease, reflecting the temperature sensitivity of the network and melting of "weak" fibrillar structures, building the network. Further heating caused a steep drop in $G*$ which is associated with the massive melting of the fibrils and network destruction. Unlike the individual gelator gels, $G*$ versus temperature plot on heating for the HSA/Mil-PCM gel manifests a two-step drop of the modulus. These steps could be associated with the melting of the networks formed by each gelator.[50] Considering the $G*$ value after completing the first drop (at ~50 °C), the step is associated with melting of the Mil network. Accordingly, the second $G*$ drop is associated with the melting of the network formed by HSA in the presence of Mil. This network appeared a little bit weakened and less thermostable as compared with the network formed in the single-gelator HSA-PCM gel of the same effective concentration, as evidenced by its slightly lower modulus and melting temperature.

The strength of the gels was characterized by the oscillatory stress amplitude sweep test (Figure 9d). This type of test is very sensitive to any change in the material structure under deformation and can distinguish the contributions of different levels of material organization.[51,52] At low-stress amplitudes, the modulus of the gels was constant and independent of the stress amplitude, indicating structural stability. An abrupt modulus drop took place when a certain critical value of the stress amplitude was exceeded. This stress amplitude is considered the yield stress, τ_y, and reflects the strength of a material's structure. The Mil-PCM gel had a τ_y of 320 Pa, which was significantly lower than that of the HSA-PCM gel (τ_y = 1000 Pa). For the HSA/Mil-PCM gel, τ_y was determined

to be 3800 Pa, a value that significantly exceeds those of the HSA- and Mil-PCM gels with the same total gelator concentration, thus confirming the synergistic effect of the gelators' blend. For the HSA/Mil-PCM gel, the presence of single yield stress was detected, whereas, for systems comprising two independent networks with different strengths, two distinctive τ_y are expected. It appears that upon formation the two networks (formed by HSA and Mil) support each other and, being subjected to shear deformations, work as a comprehensive unit.

The presence of the carbonaceous fillers affected the gelation of the HSA/Mil-blended gelator gel (SSPCM), altering the morphology (density) of the network formed by the gelator at the mesoscopic level. Both types of particles acted as nucleating agents, shifting the gelation onset temperature toward a little bit higher temperature: ~0.5° and ~1.0 °C shift was observed for SSPCM containing MWCNTs and GnPs, respectively (Figure 10). The kinetics of gelation associated
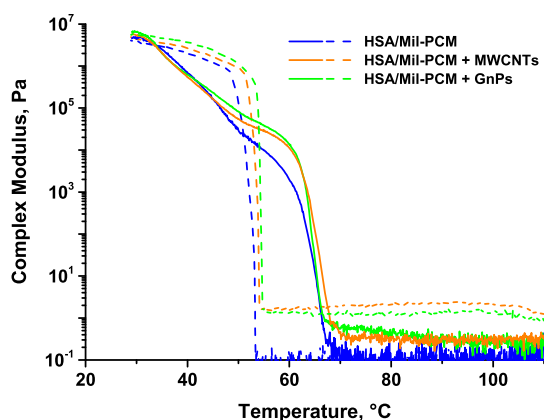
Figure 10. Typical dependences of the complex modulus vs temperature during cooling and heating stages for the SSPCM (HSA/Mil-PCM gel) and composite SSPCMs.

with the formation of the Mil network was accelerated, and the slope of the corresponding G^* versus T segments was increased. Similar to unfilled SSPCM, incubation at 30 °C was necessary for the composite SSPCMs to complete equilibrium network formation. The process, accompanied by G^* increase over time, was completed within 20−25 min, resulting in a 1.1−1.3-fold relative modulus increase for both composite SSPCMs. Absolute values of composite SSPCM gels' moduli in the solid-state only slightly exceeded that of the unfilled SSPCM (1.2- and 1.4-fold enhancement for the composite SSPCM containing MWCNTs and GnPs, respectively). On heating, a substantial effect of the carbonaceous fillers was observed in the temperature range of ~50−60 °C (see Figure 10) where the Mil-formed network is partially destroyed and only HSA and the "strongest" Mil fibrils are still present. In this region, G^* of composite SSPCMs exceeded 4− 5 times that of the unfilled SSPCM. This result is consistent with that reported in ref 53, where it is shown that the degree of mechanical properties improvement induced by the incorporation of fillers into a liquid-crystalline matrix increases with the decrease of the matrix order. The carbonaceous fillers slightly affected the thermal stability of the SSPCM, causing melting temperature growth by ~1.0° and 1.5 °C for SSPCM filled with MWCNTs and GnPs, respectively. Only a limited effect exerted by the fillers on the thermal and mechanical

properties of SSPCM can be ascribed to the low affinity of the gelators to the fillers, as strong specific interactions between the two usually lead to remarkable improvement of the properties even at lower filler concentrations.[54,55]

Enhancement of gels' strength by the introduction of fillers is a well-known phenomenon reported for many hydro- and organogels.[56,57] The gelator and the filler form two networks that support each other, which increases the yield stress of the composite gel. A similar effect was observed for GnPs containing composite SSPCM. Particularly, a ~1.4-fold yield stress growth was registered for the composite SSPCM compared with that of unfilled SSPCM (5.3 vs 3.8 kPa). Unexpectedly, the yield stress of the MWCNT containing composite SSPCM was ~20% lower than that of the unfilled SSPCM, indicating the overall weakening of the structure. Possibly, both HSA and Mil dissolved in the PCM may be absorbed and immobilized on the surface of MWCNTs and within their aggregates. Moreover, HSA and Mil molecules may differ in their absorption and immobilization propensity. Thus, at least part of the gelator molecules will not be involved in the corresponding network building upon cooling. Besides, the synergetic proportion of the blended gelator composition may be violated. As a result, the yield stress, which depends on the gelator concentration, will decrease. Though the structure formed by MWCNTs strengthens the network built by the gelators in the composite SSPCM, this contribution does not compensate for the loss of the strength caused by the alteration of the network formed by the gelators. The same reasons may explain the excess leakage observed in the composite gel.

2.2.5. Melting Crystallization Behavior. Differential scanning calorimetry (DSC) experiments were carried out to examine the melting crystallization behavior of the neat, shape-stable, and composite PCMs. Figure 11a,b shows thermograms of the neat PCM and SSPCM on cooling and the second heating. The cooling thermograms show strong exothermal effects associated with the crystallization of the PCM (see Figure 11a). The crystallization peak of the neat PCM is characterized by onset temperature $T_{c\ onset}$ = 24.8 °C and end temperature $T_{c\ end}$ = 20.9 °C, with a peak T_c = 24.8 °C. The latent heat of crystallization, ΔH_c, was 204.1 J/g. Massive heat release during neat PCM crystallization impeded proper recording of the exothermal peak, causing the sample temperature rise and the appearance of a "hook" on the crystallization peak. The second heating thermograms show endothermal peaks associated with the melting of the PCM (see Figure 11b). The melting peak of the neat PCM is characterized by onset temperature $T_{m\ onset}$ = 26.3 °C and end temperature $T_{m\ end}$ = 30.6 °C, with a peak, T_m, at 28.4 °C. The heat of fusion, ΔH_m, was 203.7 J/g, quite close to the corresponding heat released during PCM crystallization.

Gelation of the PCM did not significantly affect its crystallization (Table S2) and only slightly, by 1.2 °C, delayed the onset of the process. The heat released during the gelled PCM crystallization was 174.8 J/g, close to the value of 173.5 J/g calculated according to the PCM weight fraction in the SSPCM. The effect of gelation on the PCM melting was also insignificant. The heat of melting was 173.8 J/g, again in good agreement with the calculated value. The observed closeness between the measured values of the melting crystallization latent heats and those calculated according to the additivity rule was previously reported for polar organic PCMs gelled by a DBS derivative[14] and indicated that the gelled PCM is able to preserve its crystalline structure mainly intact. As compared
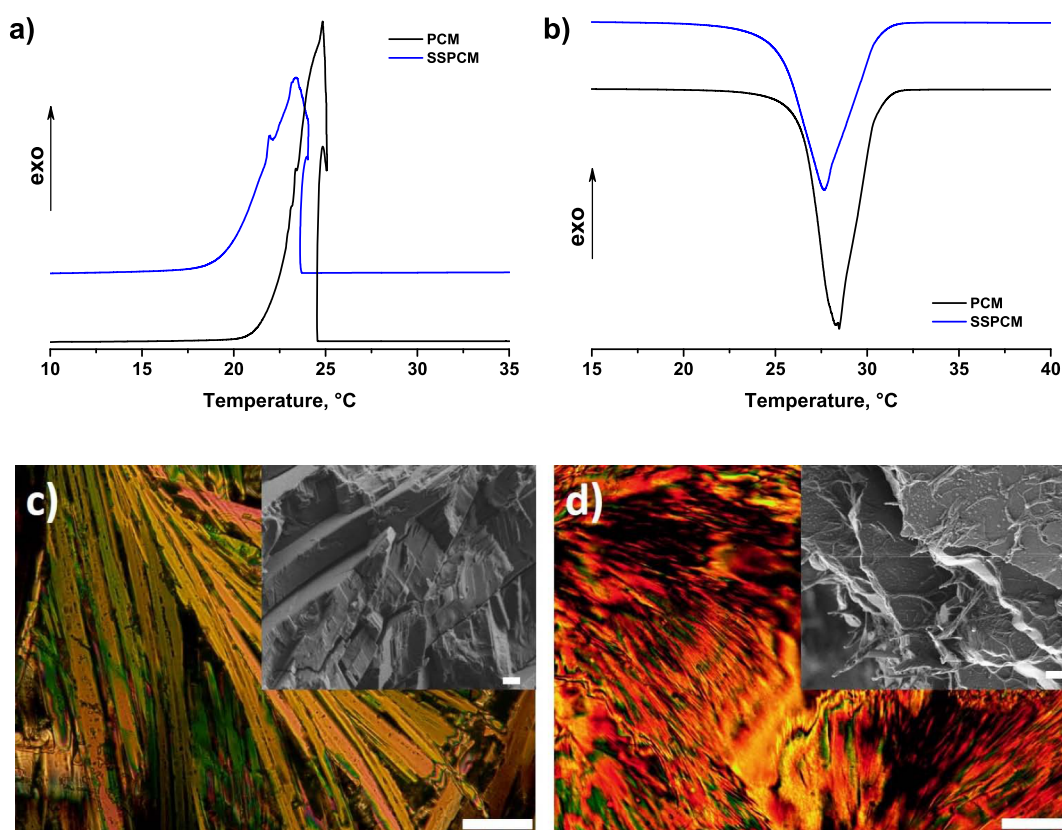
Figure 11. DSC thermograms of neat PCM and SSPCM obtained on (a) cooling and (b) second heating. Heating and cooling rates are 3 °C/min. Typical PLM images of the crystalline structure of (c) neat PCM and (d) SSPCM (scale bars represent 50 μm). Insets show cryo-SEM images of the layered structure (scale bars are 1 μm).
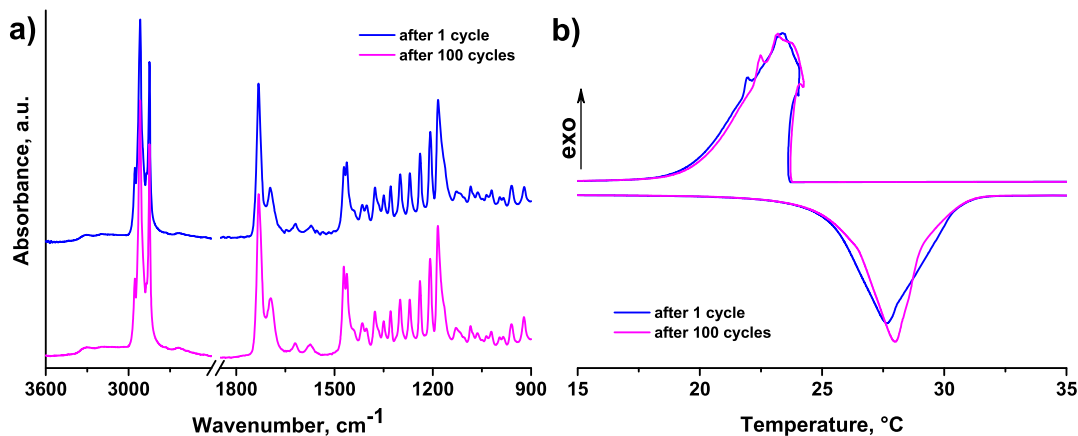
Figure 12. (a) FTIR spectra and (b) DSC thermograms obtained on cooling and heating for HSA/Mil-PCM after 1 and 100 heating−cooling cycles.

with neat PCM, an insignificant (0.9 °C) shift of SSPCM melting peak toward low temperatures is observed, indicating the PCM crystallites' size reduction. On crystallization, neat PCM formed layered structures with a layer thickness of several microns (Figure 11c). These layers possibly have a hierarchical structure, being composed of still thinner layers. Crystallized SSPCM also has a layered structure (Figure 11d). Comparative analysis of the polarized light microscopy (PLM) images reveals the structure building layers in SSPCM being much thinner than those in the neat PCM, well oriented and parallel to each other (see Figure 11d). The presence of a dense continuous network in the SSPCM likely introduces

constraints during PCM crystallization, providing a preferential direction for growing PCM crystallites and limiting their size. The growing crystallites interact with the fibrillar network formed by the gelator, partially aligning with the fibrils, rejecting and partially fracturing them, separating fragments of the network, and creating gelator-enriched domains. These domains prevent the merging of thin layers into thicker ones, as likely occurring in pure PCM. As a result, the structure observed in the SSPCM consists of thin PCM layers separated by rejected gelator fibrils concentrated on their surface (inset in Figure 11d).
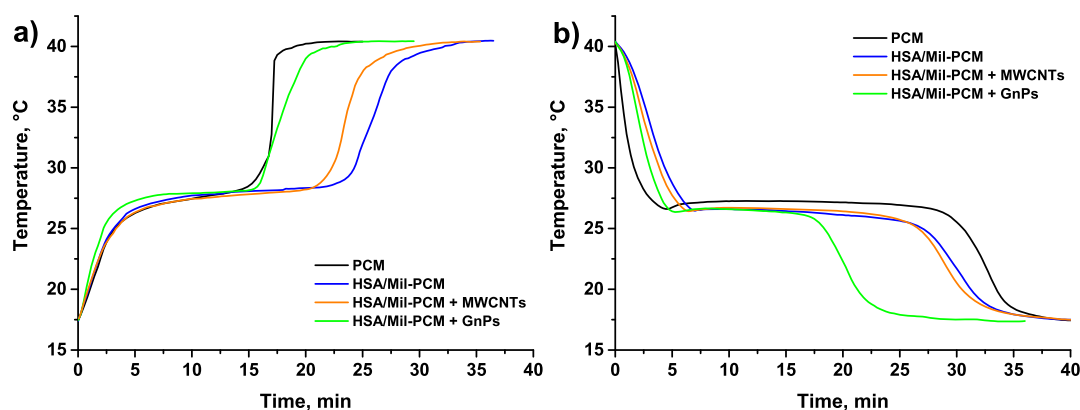
Figure 13. Evolution of temperature over time during (a) second heating and (b) cooling of PCM, SSPCM, and composite SSPCMs.

Incorporation of the fillers into the SSPCM did not significantly affect the melting crystallization behavior of the PCM as tested by DSC (Figure S2 and Table S2). The melting temperature and the heat of melting in the composite SSPCMs remained almost unchanged. The crystallization onset shifted slightly to higher temperatures due to the nucleation effect of the fillers,[58] and the heat released during PCM crystallization decreased by less than 1%.

2.2.6. Stability at Thermal Cycling. The long-term stability of the crystalline structure and chemical composition of PCMs subjected to multiple melting crystallization transitions is an important aspect because it determines their thermal performance stability and, hence, the reliability and functional lifespan. Thermal cycling by applying successive heating–cooling steps is widely used for evaluating the thermal reliability of PCMs. For evaluating the thermal cycling stability of the SSPCM, the DSC procedure, including consecutive steps of heating a sample up to 42 °C followed by its cooling down to 10 °C at a heating/cooling rate of 5 °C/min, was constructed and repeated 100 times. To guarantee the completion of the phase transition, the temperature ramp steps were separated by thermal equilibration of the sample for 2 min at the final temperature of each step. To characterize the stability of the SSPCM chemical structure, FTIR spectra were recorded for a sample after a single cycle (referred here as before cycling) and for a sample after 100 thermal cycles (Figure 12a). The corresponding DSC thermograms of the first and 100th thermal cycles are shown in Figure 12b. SSPCM gel FTIR spectra before and after thermal cycling are practically identical, and all characteristic bands are present. Because no new bands are observed, it is suggested that no changes took place in the chemical composition of the SSPCM subjected to the thermal treatment. The corresponding DSC thermograms of the original and thermally cycled samples also do not differ significantly. Usually, thermal properties of organic PCMs, subjected to thermal cycling remain unchanged, and up to 5% heat of fusion/crystallization decrease is considered acceptable.[59−63] In the case of HSA/Mil-PCM, only minor variations (0.2−0.3 °C) of phase transition peak temperatures were observed, whereas no heat of fusion/crystallization decrease was found. It should be mentioned that while the shapes of the crystallization peaks before and after cycling were similar, the corresponding melting peaks progressively narrowed with cycles, reflecting narrowing of the crystallites' size distribution.

2.2.7. Thermal Performance. The capability of the SSPCM and composite SSPCMs to store and release thermal energy during the phase transitions was examined by a simplified *T*-history test. Figure 13 presents the evolution of temperature inside the materials' bulk overheating and cooling. Each curve can be divided into three regions. At the first stage of solid material heating, a rapid linear rise of temperature is observed (Figure 13a). Increasing the temperature indicates storing of the sensible heat by the samples. The slope of the temperature versus time segment at this stage reflects the rate of sensible heat accumulation and is mostly determined by the TC of the samples and their heat capacity. The slopes of the curves for neat PCM, SSPCM, and composite SSPCM containing MWCNTs differ insignificantly (∼1.5% variation), suggesting no substantial change in either TC or heat capacity. In contrast, significantly higher, compared to the neat PCM, the slope of this segment was determined for the composite SSPCM containing 3.0 wt % of GnPs, indicating improvement of the TC. Assuming no significant difference in heat capacities of the tested samples, the observed variations of their behavior in the *T*-history tests are interpreted in terms of the TC and overall heat transfer. Following this assumption, comparison of the slopes gave ∼35% enhancement in TC for the composite SSPCM containing 3.0 wt % of GnPs. Note, that this results should be considered as an estimation.

Further heating causes the temperature−time curves to level off, reflecting the onset of melting transition. During melting, the PCM absorbs large amounts of thermal energy in the form of latent heat and the temperature remains almost constant until the phase transition process is completed. At this stage, the contribution of natural convection to the heat transfer increases with the increase of the fraction of liquid PCM. On the other hand, the extent of natural convection decreases with the decrease in the mobility of units involved in the process. In other words, the efficiency of the convection strongly deteriorates when molten PCM is immobilized by the gelator network and/or by filler particles, and the overall viscosity of the system is very high. For this reason, in the case of SSPCM gel, the plateau corresponding to PCM melting was extended in time ∼1.7-fold as compared with that of neat PCM. For composite SSPCMs, the plateau is shortened because of increased TC. Especially prominent shortening is observed in the case of composite SSPCM containing GnPs. Melting temperatures for all of the materials lie in the range of 26.9−28.3 °C, in good agreement with the values determined by DSC.

On completion of the melting transition, after PCM entirely transformed into low viscosity fluid, the contribution of natural

Table 1. TC of PCM, SSPCM, and Composite SSPCMs

		TC enhancement, %	
sample	TC, W/(m•K)	related to PCM	related to HSA/Mil-PCM
PCM	0.276 ± 0.010	0	
HSA/Mil-PCM	0.327 ± 0.002	18.4	0
HSA/Mil-PCM + MWCNTs	0.330 ± 0.007	19.6	0.9
HSA/Mil-PCM + GnPs	0.454 ± 0.042	64.5	38.8

convection to the total heat transfer is maximal, and the slope of the curve for neat PCM again increased sharply. Because SSPCMs are highly viscous systems, natural convection is not so efficient, and the temperature inside the samples during the third heating stage rises slower (slope of the third segment is lower) than in the case of neat PCMs.

Similar trends in the temperature versus time dependencies, but in reverse order, are observed during the cooling of the samples (Figure 13b). A rapid temperature decrease takes place at the first stage of cooling molten samples. The slope of the first cooling segment for the neat PCM is the highest caused by its lowest viscosity. The corresponding slopes for SSPCMs are significantly lower and differ from each other in accordance with the TC of the molten materials.

The temperature decrease continues until crystallization onset. Crystallization of neat PCM was initiated at 26.6 °C. Then, a minor temperature rise to 27.2 °C is observed, followed by a constant temperature plateau. In other words, crystallization begins only after the temperature decreases below the phase transition temperature. This means that neat PCM demonstrates crystallization with supercooling, caused by the low nucleating rate,[64] and the degree of supercooling is 0.6 °C. SSPCM and both composite SSPCMs demonstrate similar behavior with slightly lower supercooling (0.2−0.3 °C), implying that gelation and incorporation of the carbonaceous fillers accelerate nucleation of the PCM. During crystallization, the temperature remains almost constant, reflecting the release of the phase transition latent heat. The crystallization temperature was practically the same, 26.6−26.7 °C, for SSPCM and both composite SSPCMs. It should be mentioned that the melting and crystallization temperatures for the neat PCM nearly coincided, while the latter for SSPCMs was ∼1 °C lower than their melting points, suggesting the slowing of the PCM crystal growth rate in the SSPCMs.[64] The duration of the PCM crystallization process is estimated as the length of the plateau segment on the temperature−time curves and is varied for different materials. The shortest crystallization duration of composite SSPCMs containing GnPs is possibly associated with its highest solid-state TC, allowing effective heat exchange between the still molten PCM in the interior part of the container and a cold water bath surrounding the solid PCM layer formed next to container walls. The lowest solid-state conductivity of neat PCM results in the longest crystallization duration. The experimentally observed reduced melting/crystallization time of composite SSPCM containing GnPs implies its ability to store/release heat more rapidly in practical energy storage applications.

2.2.8. Thermal Conductivity. The TC measurements for pure PCM, SSPCM, and composite SSPCMs were conducted, and the results of the measurements are summarized in Table 1. TC value of the pure PCM was determined to be 0.276 W/(m•K), which belongs in the range of 0.15−0.3 W/(m•K) reported for many organic PCMs.[65] Gelation of PCM caused an 18.4% TC increase that could be ascribed to the formation

of a percolated crystalline fibrillar structure by the gelators. Incorporation of MWCNTs did not affect the TC of the SSPCM and only light, ∼1.0%, enhancement of TC is registered. This finding for composite SSPCM containing MWCNTs is surprising because the concentration used (0.6 wt %) is definitely above the percolation threshold (see Figure 4). Possibly, the dispersion of the carbon nanotubes was not good enough to realize the potential of the filler in TC enhancement, as many authors reported the enhancement of TC for 1 wt % CNT composite PCMs, which varied within a wide range ∼6− 170%.[22,60,66−68] Oppositely, a significant rise of TC was observed for SSPCM containing 3.0 wt % GnPs; the TC value was equal to 0.454 W/(m•K), which is ∼40% higher than the value obtained for unfilled SSPCM. Thus, the overall effect of TC enhancement caused by both gelation and incorporation of graphene nanoparticles reached 64.5%. Similarly, an increase of TC for PCMs filled with 3 wt % of GnPs is reported to vary in a range of ∼30−300% due to the differences in the dispersion state of GnP particles and their size.[13,22,60,69] Note, that the estimation of TC improvement based on the results of T-history tests gave underestimated values when compared with those obtained by direct TC measurements.

2.2.9. Thermal Stability. The thermal stability of the materials under consideration was examined by thermogravimetric analysis (TGA). Figure 14 shows the materials weight
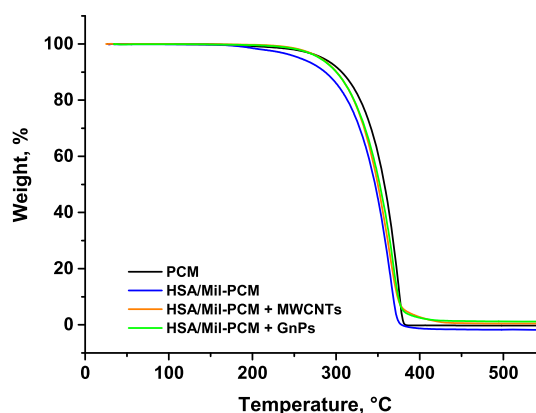

Figure 14. TGA curves of PCM, SSPCM, and composite SSPCMs.

loss during heating. Thermal degradation of the neat PCM occurs in one step within the temperature range of 230−380 °C. The characteristic temperature corresponding to 10% weight loss, T_{10}, is 305 °C. Unfilled SSPCM loses 10% of its weight at a lower temperature, T_{10} = 287 °C, with the highest weight loss rate (peak in weight loss derivative plot) at 365 °C, quite close to the value reported at 355 °C for the pure HSA.[70] For both composite SSPCMs, T_{10} lies in between the corresponding values for neat PCM and unfilled SSPCM. The thermal degradation onset temperature is significantly
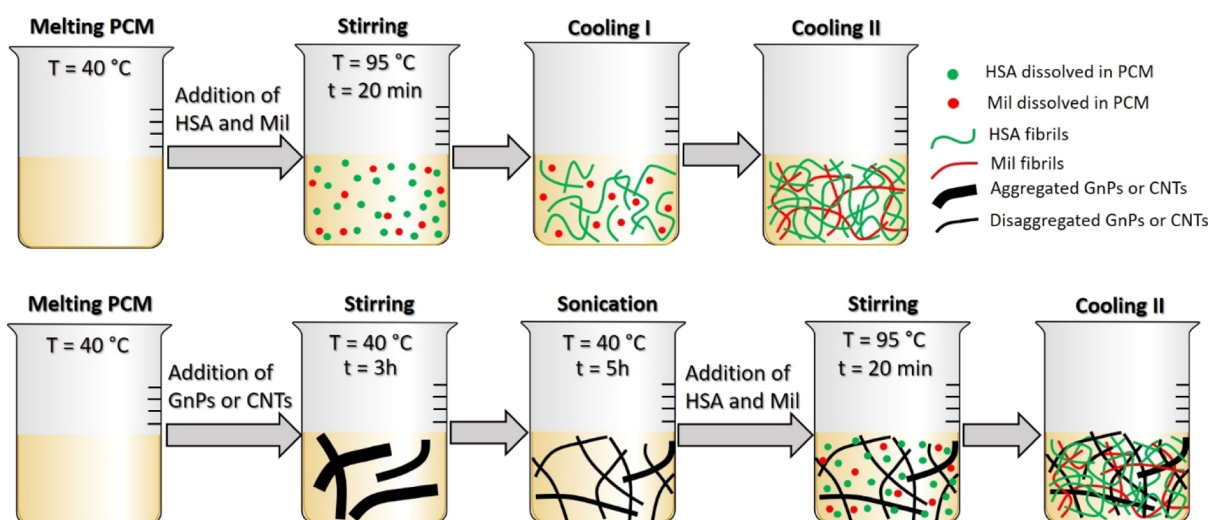
Figure 15. Step-by-step preparation of (upper row) HSA/Mil-PCM and (bottom row) composite PCM gels. For the latter, cooling step I is skipped.

higher than the working temperature, so the thermal stability of all the materials is adequate for potential applications.

3. CONCLUSIONS

Two organogelators of different chemistries, that is, a derivative of fatty acid (HSA) and a derivative of bis-urea (Mil), and their blend with a HSA/Mil synergetic ratio of 83/17, were shown to be capable of gelling an ambient temperature, bio-based (fatty acid-derived) PCM. Gelation of the PCM has not significantly affected its melting crystallization behavior. However, the presence of the gel network affected the crystalline morphology of the PCM. The gelled PCM showed stacked structures composed of alternating PCM layers separated by layers formed by gelator fibrils. The HSA/Mil gelator at a concentration of 15 wt % eliminates leakage of the liquid PCM. The 15 wt % HSA/Mil-PCM gel demonstrated 18.4% TC enhancement together with the stability of the chemical composition, crystalline structure, and thermal performance during multiple thermal cycles. Testing the further possibility of TC improvement, MWCNTs and graphene platelets were incorporated in the gel at concentrations exceeding the corresponding percolation thresholds. The presence of the carbonaceous fillers has not altered the melting crystallization behavior of the gelled PCM. Incorporation of the nanotubes has not resulted in TC enhancement of the SSPCM gel. Moreover, strength reduction and excessive PCM leakage were observed. On the other hand, graphene addition caused a ~40% TC increase along with ~1.5-fold strength growth. No excessive PCM leakage was detected in the graphene containing composite SSPCM. The presence of the graphene platelets caused a significant acceleration of phase transitions in the composite SSPCM, as detected by the T-history test and an overall ~65% TC increase. The ability of more rapid thermal energy storing/releasing processes, resulting from the accelerated phase transitions, makes the graphene-containing composite SSPCM attractive for practical ambient temperature thermal energy storage applications like solar-thermal installations, temperature-controlled greenhouse, and water heating systems.

4. EXPERIMENTAL SECTION

4.1. Materials. The bio-based CrodaTherm 29-SO-(GD) PCM, a proprietary organic phase change material derived from plant-based feedstocks, was purchased from Croda International (UK). According to the data provided by the manufacturer, it is a fatty acid-derived material.

Gelling agent 12-hydroxystearic acid (HSA) was purchased from Sigma Aldrich (Rehovot, Israel). Gelling agent Millithix MT-800 (Mil) is a proprietary bis-urea derivative, bis-(C_{12-14} alkyl propyleneglycol-4)hexamethylenediurea was kindly provided by Milliken Chemical (USA).

GnPs (H-15 grade, XG-Sciences Inc., USA), used in this study, are characterized by mean lateral dimensions of 20 ± 5 μm, an aspect ratio of 560 ± 300, and a low defect density of 0.07.[71] MWCNTs, according to the information provided by the manufacturer (INP, Toulouse, France), have a diameter of 10−20 nm, a length of ≥10 μm, and a specific area of 700−1000 m^2/g. MWCNT powder contains 95 vol % of nanotubes.

4.2. Preparation of Gels. The gels were prepared by melt blending the PCM with an appropriate amount of gelling agents at ~95 °C (boiling water bath) for 20 min using a magnetic stirrer, followed by cooling at ambient conditions (20−22 °C). The concentration of the gelling agents varied within the range of 3−15 wt %. The gels containing the HSA and Mil blend at a fixed HSA/Mil ratio of 83/17 wt % were prepared in the same way. In this case, powders of the individual gelators were first premixed, and then dissolved in the molten PCM. The blended gelator concentration range was 1.0−15 wt %. For composite gel preparation, the corresponding amount of the filler, either GnPs or MWCNTs, was added to the molten PCM at 40−45 °C, stirred for several hours using a magnetic stirrer, and then additionally homogenized in a Delta D-80 sonication bath (80 W, 43 kHz) at 40 °C for 5 h. After that, gels were prepared following the same protocol as described for the gels without fillers. The concentration of the fillers in the composite gels varied between 0.2−0.6 wt % and 0.5−3.0 wt % for MWCNTs and GnPs, respectively. Figure 15 illustrates a step-by-step preparation of the blended gelator, HSA/Mil, and composite gels.

4.3. Methods of Characterization. A Nicolet 380 (Thermo Scientific, USA) FTIR spectrometer was used to obtain information about the chemical structure of materials. The spectrum was collected in the range of 600–4000 cm^{-1}, with 0.5 cm^{-1} resolution.

A Discovery DHR-2 rotational rheometer (TA Instruments, USA) was used to study the rheological properties of the gels under the oscillatory shear deformation mode. Parallel plate geometry with a diameter of 40 mm and a gap of 0.4 mm was applied. The plates with rough, sandblasted surfaces were used to prevent slipping. In order to characterize thermo-mechanical properties of the gels, the procedure, consisting of several steps, was developed. First, the sample was heated to 110 °C, a temperature well above the gel–sol transition temperature, and then extensively sheared to remove the influence of thermal prehistory. Then, the solution was cooled to 30 °C at a cooling rate of 3 °C/min, then incubated at this temperature for 35 min, and heated again to 110 °C at the same heating rate of 3 °C/min. Changes in storage and loss moduli with the temperature were recorded. Under the selected experimental conditions, all the tested materials showed linear viscoelastic behavior over the entire temperature range. The measurements were done in triplicate and mean values of the complex dynamic modulus and phase transition temperatures were determined. The viscosity of the molten gels and suspensions containing MWCNTs or GnPs was measured under steady-state shear deformation in a control rate mode using the parallel plate geometry with a diameter of 40 mm and a smooth untreated surface.

The PCM leakage was measured by the filter sheet-sandwich method.[6] Cylindrical samples with a diameter of 25 mm and a height of ∼12 mm (the weight of the samples was ∼4 g) were placed onto a sandwich of filter sheets and incubated at 42 °C for 2 h. The filter sheets were weighed before and after the incubation stages. The leakage of the PCM was calculated as

$$\text{leakage} = \frac{(M_2 - M_1)}{W \cdot c} \cdot 100\%$$

where M_1 and M_2 are the weights of the filter sheets before and after the incubation stage, respectively; W is the weight of the sample; and c is the concentration of the PCM in the sample. For the formulation with the highest (15 wt %) concentration of the HSA/Mil gelator and for composite gels with the highest filler content (0.6% of MWCNTs and 3.0% of GnPs), the measurements were done in triplicate and the mean values are presented.

An Olympus BX51-P light microscope was used to characterize the morphology of the prepared gels. Gel anisotropy was examined using PLM. A small piece of the gels was placed between two glass plates, heated to 110 °C to melt the structure, and then cooled to 30 °C at a constant rate of 3 °C/min. The edges of the glass plates were sealed with silicone grease to prevent molten PCM leakage and evaporation.

A Zeiss Ultra Plus high-resolution scanning electron microscope equipped with a Schottky field-emission gun and with a BalTec VCT100 cold stage, maintained at a temperature below −145 °C, was used for the nanostructural morphological characterization of the gels by cryogenic scanning electron microscopy (cryo-SEM) imaging. Specimens were imaged at a low acceleration voltage (1.2–1.4 kV) and working distances of 3–5 mm. Everhart Thornley ("SE2") and the in-the-column ("inLens") secondary electron detectors were used. The

structures emerged and were exposed during the examination, most probably due to the gentle local matrix selective sublimation caused by the electron beam scanning over the sample surface. The specimens were prepared by mounting a piece of the gel on a dedicated stab, which was then immersed in liquid nitrogen. The frozen specimen was then screwed onto a specialized liquid nitrogen-cooled sample table and transferred via a high vacuum cryo-transfer shuttle (VCT100; Bal-Tec) to a freeze-fracture system (BAF060; Leica), where it was maintained at −170 °C. The frozen samples were fractured by the rapid impact of a cooled knife, exposing their brittle fractured surface. The fractured samples were then transferred to a pre-cooled high-resolution scanning electron microscope. Imaging was performed as close as possible to the fractured surface, where the cooling rate is expected to be maximal.

The microstructure of the pure PCM and the gels was characterized by SAXS, using a small-angle diffractometer (Molecular Metrology SAXS system, JJ X-ray A/S, Hørsholm, Denmark), with Cu Kα radiation (λ = 0.1542 nm), and a generator powered at 45 kV and 0.9 mA. A DHR-2 rheometer was used for sample preparation. The samples were prepared according to the same protocol and was used for the rheological characterization of the gels, including melting, shearing, cooling, and incubation stages. Finally, the formed gels were cooled to 20 °C at a cooling rate of 3 °C/min. X-ray measurements were taken at 20 °C, under vacuum.

A Discovery DSC-2500 differential scanning calorimeter (TA Instruments, USA) was used to characterize the thermal behavior of the gels. The tests were conducted at a constant heating or cooling rate of 3 °C/min. TRIOS software was used to analyze the data. The phase transition temperatures and the corresponding heat of fusion/crystallization were determined as the temperature at the peak position of the normalized heat flow versus the temperature curve and the integrated area of the peak and the interpolated baseline between the beginning and end of the phase transition, respectively. The DSC experiments were repeated for some of the samples; it was found that peak positions and heat of fusion/crystallization were reproducible with the standard deviations of ±0.2 °C and ±1.1 J/g, respectively, values which could be considered as negligible.

A simplified T-history test[72] was carried out to characterize the thermal energy storage performance of the materials. Briefly, a container with a sample (∼5 g) and a thermocouple (K-type) sealed in the middle of its bulk was immersed in a cold water bath. After ∼20 min of soaking, when the temperature stabilized at 17.5 °C, the container was quickly transferred to a high-temperature water bath preheated at 42 °C. After equilibration at this temperature, the container was transferred back to the cold water bath. Temperature evolution inside the bulk during the heating–cooling–heating processes was recorded by a data sampler (Pico TC-08). The melting/crystallization temperatures were determined as the temperatures at the curve portions where the temperature was constant over time. The time, corresponding to the beginning and end of phase transitions, was determined using onset point and endset point procedures, respectively.

TC was measured by a thermal constant analyzer (Hot Disk TPS 2500S, Sweden) based on a transient plane source—an electrically conducting double-spiral shaped nickel foil sandwiched between two thin sheets of an insulating material (Kapton). When performing a TC measurement, a plane hot disk sensor (2.001 mm Kapton sensor 7577) was placed

between two disc-like samples with a diameter of 25 mm and 4−6 mm in thickness. During heating, the sensor measured the temperature increase inside the sample over time. Measurement time and power output of the sensor was varied from sample to sample. By controlling the probing depth (i.e., the distance between the sensor and the sample boundaries) and the total to characteristic (TTC) parameter (i.e., the relation between diffusivity, measurement time, and radius of the sensor), we optimize the measurement condition and prevent convection or radiation from the sample boundaries. The time-dependent change in the temperature was used to calculate the TC of the materials. The measurements were repeated three times for each sample.

TGA (TGA/DSC-3+, Mettler Toledo, Switzerland) was carried out to determine the decomposition temperature. The tests were conducted in the temperature range of 25−550 °C at a heating rate of 20 °C/min under a nitrogen atmosphere.

■ ASSOCIATED CONTENT

Ⓢ Supporting Information

The Supporting Information is available free of charge at https://pubs.acs.org/doi/10.1021/acsomega.1c07376.

> FTIR spectra; DSC thermograms; heat and temperatures of phase transitions; and leakage of molten PCM in SSPCM and composite SSPCMs (PDF)

■ AUTHOR INFORMATION

Corresponding Authors

Gleb Vasilyev − *Faculty of Mechanical Engineering, Technion—Israel Institute of Technology, Haifa 32000, Israel;* ⓘ orcid.org/0000-0002-7229-0196; Email: mevasil@technion.ac.i.l

Eyal Zussman − *Faculty of Mechanical Engineering, Technion—Israel Institute of Technology, Haifa 32000, Israel;* Email: meeyal@technion.ac.il

Authors

Naama Koifman − *Faculty of Chemical Engineering, Technion—Israel Institute of Technology, Haifa 32000, Israel*

Michael Shuster − *Carmel Olefins Limited—BAZAN Group, Haifa 31014, Israel*

Michael Gishvoliner − *Carmel Olefins Limited—BAZAN Group, Haifa 31014, Israel*

Yachin Cohen − *Faculty of Chemical Engineering, Technion—Israel Institute of Technology, Haifa 32000, Israel*

Complete contact information is available at:
https://pubs.acs.org/10.1021/acsomega.1c07376

Author Contributions

All authors participated in the writing of this manuscript. All authors have given approval for the final version of the manuscript.

Notes

The authors declare no competing financial interest.

■ ACKNOWLEDGMENTS

■ REFERENCES

(1) Pielichowska, K.; Pielichowski, K. Phase change materials for thermal energy storage. *Prog. Mater. Sci.* **2014**, *65*, 67−123.

(2) Umair, M. M.; Zhang, Y.; Iqbal, K.; Zhang, S.; Tang, B. Novel strategies and supporting materials applied to shape-stabilize organic phase change materials for thermal energy storage-A review. *Appl. Energy* **2019**, *235*, 846−873.

(3) Jelle, B. P.; Kalnæs, S. E. Phase Change Materials for Application in Energy-Efficient Buildings. In *Cost-Effective Energy Efficient Building Retrofitting: Materials, Technologies, Optimization and Case Studies*; PachecoTorgal, F., Granqvist, C. G., Jelle, B. P., Vanoli, G. P., Bianco, N., Kurnitski, J., Eds.; Woodhead Publication Ltd.: Cambridge, 2017; pp 57−118.

(4) Zhang, X.; Deng, P.; Feng, R.; Song, J. Novel gelatinous shape-stabilized phase change materials with high heat storage density. *Sol. Energy Mater. Sol. Cells* **2011**, *95*, 1213−1218.

(5) Chen, F.; Wolcott, M. Polyethylene/paraffin binary composites for phase change material energy storage in building: A morphology, thermal properties, and paraffin leakage study. *Sol. Energy Mater. Sol. Cells* **2015**, *137*, 79−85.

(6) Beginn, U. Applicability of frozen gels from ultra high molecular weight polyethylene and paraffin waxes as shape persistent solid/liquid phase change materials. *Macromol. Mater. Eng.* **2003**, *288*, 245−251.

(7) Xiao, M.; Feng, B.; Gong, K. Thermal performance of a high conductive shape-stabilized thermal storage material. *Sol. Energy Mater. Sol. Cells* **2001**, *69*, 293−296.

(8) Zhang, Y. P.; Lin, K. P.; Yang, R.; Di, H. F.; Jiang, Y. Preparation, thermal performance and application of shape-stabilized PCM in energy efficient buildings. *Energy Build.* **2006**, *38*, 1262−1269.

(9) Song, G.; Ma, S.; Tang, G.; Yin, Z.; Wang, X. Preparation and characterization of flame retardant form-stable phase change materials composed by EPDM, paraffin and nano magnesium hydroxide. *Energy* **2010**, *35*, 2179−2183.

(10) Wu, W.; Wu, W.; Wang, S. Form-stable and thermally induced flexible composite phase change material for thermal energy storage and thermal management applications. *Appl. Energy* **2019**, *236*, 10−21.

(11) Wu, B.; Zhao, Y.; Liu, Q.; Zhou, C.; Zhang, X.; Lei, J. Form-stable phase change materials based on castor oil and palmitic acid for renewable thermal energy storage. *J. Therm. Anal. Calorim.* **2019**, *137*, 1225−1232.

(12) Shuster, M.; Gishboliner, M.; Shemesh, R. Thermoplastic Shape-Stable Polymer Compositions for Storing Thermal Energy. WO 2020129038 A1, 2020.

(13) Saeed, R. M.; Schlegel, J. P.; Castano, C.; Sawafta, R. Preparation and enhanced thermal performance of novel (solid to gel) form-stable eutectic PCM modified by nano-graphene platelets. *J. Energy Storage* **2018**, *15*, 91−102.

(14) Niu, L.; Bai, G.; Song, J. 1,3:2,4-di-(3,4-dimethyl)benzylidene sorbitol organogels used as phase change materials: solvent effects on structure, leakage and thermal performance. *RSC Adv.* **2015**, *5*, 21733−21739.

(15) Tian, T.; Song, J.; Niu, L.; Feng, R. Preparation and properties of 1-tetradecanol/1,3:2,4-di-(3,4-dimethyl) benzylidene sorbitol gelatinous form-stable phase change materials. *Thermochim. Acta* **2013**, *554*, 54−58.

(16) Radhakrishnan, N.; Thomas, S.; Sobhan, C. B. Characterization of thermophysical properties of nano-enhanced organic phase change materials using T-history method. *J. Therm. Anal. Calorim.* **2020**, *140*, 2471−2484.

(17) Fang, G.; Yu, M.; Meng, K.; Shang, F.; Tan, X. High-Performance Phase-Change Materials Based on Paraffin and Expanded Graphite for Solar Thermal Energy Storage. *Energy Fuels* **2020**, *34*, 10109−10119.

(18) Gorbacheva, S. N.; Makarova, V. V.; Ilyin, S. O. Hydrophobic nanosilica-stabilized graphite particles for improving thermal conductivity of paraffin wax-based phase-change materials. *J. Energy Storage* **2021**, *36*, 102417.

(19) Ai, H.; Lv, L.; Chen, T.; Zhang, Y.; Dong, L.; Song, S. An eco-friendly and facile montmorillonite nanosheets aerogel based phase change materials for efficient solar-to-thermal energy conversion. *Energy Convers. Manage.* **2022**, *253*, 115172.

(20) Nadiv, R.; Shachar, G.; Peretz-Damari, S.; Varenik, M.; Levy, I.; Buzaglo, M.; Ruse, E.; Regev, O. Performance of nano-carbon loaded polymer composites: Dimensionality matters. *Carbon* **2018**, *126*, 410−418.

(21) Ohayon-Lavi, A.; Lavi, A.; Alatawna, A.; Ruse, E.; Ziskind, G.; Regev, O. Graphite-based shape-stabilized composites for phase change material applications. *Renewable Energy* **2021**, *167*, 580−590.

(22) Yu, S.; Jeong, S.-G.; Chung, O.; Kim, S. Bio-based PCM/carbon nanomaterials composites with enhanced thermal conductivity. *Sol. Energy Mater. Sol. Cells* **2014**, *120*, 549−554.

(23) Vasilyev, G.; Koifman, N.; Shuster, M.; Gishvoliner, M.; Cohen, Y.; Zussman, E. Synergistic Effect of Two Organogelators for the Creation of Bio-Based, Shape-Stable Phase-Change Materials. *Langmuir* **2020**, *36*, 15572−15582.

(24) Carr, A. J.; Melendez, R.; Geib, S. J.; Hamilton, A. D. The design of organic gelators: Solution and solid state properties of a family of bis-ureas. *Tetrahedron Lett.* **1998**, *39*, 7447−7450.

(25) Hanabusa, K.; Shimura, K.; Hirose, K.; Kimura, M.; Shirai, H. Formation of organogels by intermolecular hydrogen bonding between ureylene segment. *Chem. Lett.* **1996**, *25*, 885−886.

(26) Grahame, D. A. S.; Olauson, C.; Lam, R. S. H.; Pedersen, T.; Borondics, F.; Abraham, S.; Weiss, R. G.; Rogers, M. A. Influence of chirality on the modes of self-assembly of 12-hydroxystearic acid in molecular gels of mineral oil. *Soft Matter* **2011**, *7*, 7359−7365.

(27) Wu, S.; Gao, J.; Emge, T. J.; Rogers, M. A. Solvent-Induced Polymorphic Nanoscale Transitions for 12-Hydroxyoctadecanoic Acid Molecular Gels. *Cryst. Growth Des.* **2013**, *13*, 1360−1366.

(28) De Gennes, P.-G. *Scaling Concepts in Polymer Physics*; Cornell University Press: New York, 1979.

(29) Rogers, M. A.; Marangoni, A. G. Solvent-Modulated Nucleation and Crystallization Kinetics of 12-Hydroxystearic Acid: A Non-isothermal Approach. *Langmuir* **2009**, *25*, 8556−8566.

(30) Bui, A.; Virgilio, N. Tuning Organogel Properties by Controlling the Organic-Phase Composition. *Ind. Eng. Chem. Res.* **2013**, *52*, 14185−14191.

(31) Rogers, M. A.; Marangoni, A. G. Non-Isothermal Nucleation and Crystallization of 12-Hydroxystearic Acid in Vegetable Oils. *Cryst. Growth Des.* **2008**, *8*, 4596−4601.

(32) Lascialfari, L.; Pescitelli, G.; Brandi, A.; Mannini, M.; Berti, D.; Cicchi, S. Urea vs. carbamate groups: a comparative study in a chiral C-2 symmetric organogelator. *Soft Matter* **2015**, *11*, 8333−8341.

(33) Liu, S.; Yu, W.; Zhou, C. Solvents effects in the formation and viscoelasticity of DBS organogels. *Soft Matter* **2013**, *9*, 864−874.

(34) Terech, P.; Pasquier, D.; Bordas, V.; Rossat, C. Rheological properties and structural correlations in molecular organogels. *Langmuir* **2000**, *16*, 4485−4494.

(35) Wilder, E. A.; Hall, C. K.; Khan, S. A.; Spontak, R. J. Effects of composition and matrix polarity on network development in organogels of poly(ethylene glycol) and dibenzylidene sorbitol. *Langmuir* **2003**, *19*, 6004−6013.

(36) Jones, J. L.; Marques, C. M. Rigid polymer network models. *J. Phys.* **1990**, *51*, 1113−1127.

(37) Halperin-Sternfeld, M.; Ghosh, M.; Sevostianov, R.; Grigoriants, I.; Adler-Abramovich, L. Molecular co-assembly as a strategy for synergistic improvement of the mechanical properties of hydrogels. *Chem. Commun.* **2017**, *53*, 9586−9589.

(38) Ohsedo, Y.; Taniguchi, M.; Oono, M.; Saruhashi, K.; Watanabe, H. Long-chain alkylamide-derived oil gels: mixing induced onset of thixotropy and application in sustained drug release. *New J. Chem.* **2015**, *39*, 6482−6490.

(39) Liu, G.; Zhou, C.; Teo, W. L.; Qian, C.; Zhao, Y. Self-Sorting Double-Network Hydrogels with Tunable Supramolecular Handedness and Mechanical Properties. *Angew. Chem., Int. Ed.* **2019**, *58*, 9366−9372.

(40) Piras, C. C.; Smith, D. K. Sequential Assembly of Mutually Interactive Supramolecular Hydrogels and Fabrication of Multi-Domain Materials. *Chem.—Eur. J.* **2019**, *25*, 11318−11326.

(41) Weiss, R. G.; Terech, P. *Molecular Gels: Materials with Self-Assembled Fibrillar Networks*; Springer Science & Business Media, 2006.

(42) Li, M.; Mu, B. Effect of different dimensional carbon materials on the properties and application of phase change materials: A review. *Appl. Energy* **2019**, *242*, 695−715.

(43) Hong, Y.; Yan, W.; Du, J.; Li, W.; Xu, T.; Ye, W.-B. Thermal performances of stearic acid/sepiolite composite form-stable phase change materials with improved thermal conductivity for thermal energy storage. *J. Therm. Anal. Calorim.* **2021**, *143*, 3317−3329.

(44) Malkin, A. Y.; Isayev, A. I. *Rheology: Concepts, Methods, and Applications*, 3rd ed.; Chemtec Publishing: Toronto Scarborough, 2017; pp 1−486.

(45) Liberman, L.; Kleinerman, O.; Davidovich, I.; Talmon, Y. Micrograph contrast in low-voltage SEM and cryo-SEM. *Ultramicroscopy* **2020**, *218*, 113085.

(46) Stenhagen, E.; Vand, V.; Sim, A. The crystal structure of isopalmitic acid. *Acta Crystallogr.* **1952**, *5*, 695−696.

(47) Terech, P. Small-Angle-Scattering Study Of 12-Hydroxystearic Physical Organogels And Lubricating Greases. *Colloid Polym. Sci.* **1991**, *269*, 490−500.

(48) Koitani, S.; Dieterich, S.; Preisig, N.; Aramaki, K.; Stubenrauch, C. Gelling Lamellar Phases of the Binary System Water-Didodecyldimethylammonium Bromide with an Organogelator. *Langmuir* **2017**, *33*, 12171−12179.

(49) Terech, P.; Rodriguez, V.; Barnes, J. D.; McKenna, G. B. Organogels and Aerogels Of Racemic And Chiral 12-Hydroxyocta-decanoic Acid. *Langmuir* **1994**, *10*, 3406−3418.

(50) Fuentes-Caparrós, A. M.; de Paula Gómez-Franco, F.; Dietrich, B.; Wilson, C.; Brasnett, C.; Seddon, A.; Adams, D. J. Annealing multicomponent supramolecular gels. *Nanoscale* **2019**, *11*, 3275−3280.

(51) Ahuja, A.; Potanin, A.; Joshi, Y. M. Two step yielding in soft materials. *Adv. Colloid Interface Sci.* **2020**, *282*, 102179.

(52) Vasilyev, G. B.; Dreval', V. E.; Malkin, A. Y.; Kulichikhin, V. G. Rheology of Linear and Branched Styrene-Acrylonitrile Copolymers. Similarities and Differences. *Polym. Sci., Ser. A* **2010**, *52*, 1142−1155.

(53) Vasilyev, G. B.; Makarova, V. V.; Rebrov, A. V.; Picken, S. J.; Smirnova, N. M.; Malkin, A. Y.; Kulichikhin, V. G. Morphology and Rheology of Composites Based on Anisotropic Polymer Matrix and Different Clays. *J. Appl. Polym. Sci.* **2011**, *120*, 3642−3653.

(54) Mandal, D.; Kar, T.; Das, P. K. Pyrene-Based Fluorescent Ambidextrous Gelators: Scaffolds for Mechanically Robust SWNT-Gel Nanocomposites. *Chem.—Eur. J.* **2014**, *20*, 1349−1358.

(55) Adhikari, B.; Nanda, J.; Banerjee, A. Pyrene-Containing Peptide-Based Fluorescent Organogels: Inclusion of Graphene into the Organogel. *Chem.—Eur. J.* **2011**, *17*, 11488−11496.

(56) Moniruzzaman, M.; Sahin, A.; Winey, K. I. Improved mechanical strength and electrical conductivity of organogels containing carbon nanotubes. *Carbon* **2009**, *47*, 645−650.

(57) Tian, Y.; Zhang, L.; Duan, P.; Liu, F.; Zhang, B.; Liu, C.; Liu, M. Fabrication of organogels composed from carbon nanotubes through a supramolecular approach. *New J. Chem.* **2010**, *34*, 2847−2852.

(58) Jebasingh, B. E.; Arasu, A. V. A detailed review on heat transfer rate, supercooling, thermal stability and reliability of nanoparticle dispersed organic phase change material for low-temperature applications. *Mater. Today Energy* **2020**, *16*, 100408.

(59) Yi, H.; Zhan, W.; Zhao, Y.; Qu, S.; Wang, W.; Chen, P.; Song, S. A novel core-shell structural montmorillonite nanosheets/stearic acid composite PCM for great promotion of thermal energy storage properties. *Sol. Energy Mater. Sol. Cells* **2019**, *192*, 57−64.

(60) Wu, X.; Gao, M.; Wang, K.; Wang, Q. W.; Cheng, C. X.; Zhu, Y. J.; Zhang, F. F.; Zhang, Q. Experimental Study of the Thermal Properties of a Homogeneous Dispersion System of a Paraffin-based Composite Phase Change Materials. *J. Energy Storage* **2021**, *36*, 102398.

(61) Cárdenas-Ramírez, C.; Gómez, M. A.; Jaramillo, F.; Fernández, A. G.; Cabeza, L. F. Thermal reliability of organic-organic phase change materials and their shape-stabilized composites. *J. Energy Storage* **2021**, *40*, 102661.

(62) Song, S.; Ai, H.; Zhu, W.; Lv, L.; Feng, R.; Dong, L. Carbon aerogel based composite phase change material derived from kapok fiber: Exceptional microwave absorbility and efficient solar/magnetic to thermal energy storage performance. *Composites, Part B* **2021**, *226*, 109330.

(63) Liao, H.; Guo, S.; Liu, Y.; Wang, Q. Form-stable phase change composites with high thermal conductivity and adjustable thermal management capacity. *Sol. Energy Mater. Sol. Cells* **2021**, *221*, 110881.

(64) Garg, H. P.; Mullick, S. C.; Bhargava, A. K. Latent Heat or Phase Change Thermal Energy Storage. *Solar Thermal Energy Storage*; Springer Netherlands: Dordrecht, 1985; pp 154−291.

(65) Singh, S. P.; Bhat, V. Applications of organic phase change materials for thermal comfort in buildings. *Rev. Chem. Eng.* **2014**, *30*, 521−538.

(66) Zou, D.; Ma, X.; Liu, X.; Zheng, P.; Hu, Y. Thermal performance enhancement of composite phase change materials (PCM) using graphene and carbon nanotubes as additives for the potential application in lithium-ion power battery. *Int. J. Heat Mass Transfer* **2018**, *120*, 33−41.

(67) Harmen, Y.; Chhiti, Y.; Alaoui, F. E. M.; Bentiss, F.; Jama, C.; Duquesne, S.; Bensitel, M. Thermal performance of PEG-MWCNTs composites as shape-stabilised phase change materials for thermal energy storage. *Fullerenes, Nanotubes, Carbon Nanostruct.* **2021**, *29*, 732.

(68) Liu, C.; Zhang, X.; Lv, P.; Li, Y.; Rao, Z. Experimental study on the phase change and thermal properties of paraffin/carbon materials based thermal energy storage materials. *Phase Transitions* **2017**, *90*, 717−731.

(69) Tang, Y.; Jia, Y.; Alva, G.; Huang, X.; Fang, G. Synthesis, characterization and properties of palmitic acid/high density polyethylene/graphene nanoplatelets composites as form-stable phase change materials. *Sol. Energy Mater. Sol. Cells* **2016**, *155*, 421−429.

(70) Yang, J.; Lu, S.; Pan, L.; Luo, Q.; Song, L.; Wu, L.; Yu, J. Effect of epoxidized soybean oil grafted poly(12-hydroxy stearate) on mechanical and thermal properties of microcrystalline cellulose fibers/polypropylene composites. *Polym. Bull.* **2017**, *74*, 911−930.

(71) Ligati, S.; Ohayon-Lavi, A.; Keyes, J.; Ziskind, G.; Regev, O. Enhancing thermal conductivity in graphene-loaded paint: Effects of phase change, rheology and filler size. *Int. J. Therm. Sci.* **2020**, *153*, 106381.

(72) Zhang, Y.; Jiang, Y.; Jiang, Y. A simple method, the T-history method, of determining the heat of fusion, specific heat and thermal conductivity of phase-change materials. *Meas. Sci. Technol.* **1999**, *10*, 201−205.